ACS APPLIED MATERIALS & INTERFACES

Research Article

www.acsami.org

Controllable Fabrication of Patterned ZnO Nanorod Arrays: Investigations into the Impacts on Their Morphology

Dian-bo Zhang, Shu-jie Wang, Ke Cheng, Shu-xi Dai, Bin-bin Hu, Xiao Han, Qing Shi, and Zu-liang Du*

Key Lab for Special Functional Materials of Ministry of Education, Henan University, Kaifeng 475004, China

ABSTRACT: Fabricating ZnO nanorod arrays with precisely controlled morphology, alignment, and density is highly desirable but rather challenging. On the other hand, understanding the parameters that affect their final morphology and the growth mechanisms is significant to integrate such patterned ZnO nanorod arrays in various applications. Therefore, ZnO nanorod arrays with different density and morphology were fabricated by electron beam lithography (EBL) combined with the hydrothermal methods in this work. The influences of prepatterned geometry and the growth parameters such as seed layer, the precursor concentration, and the growth time on their final morphology were investigated. Under the coactions of EBL and the subsequent hydrothermal growth, ZnO nanorod arrays with precisely controlled density, position and morphology were achieved. The growth mechanism was also discussed in detail for the ZnO nanorod arrays which confined by the aperture with different size.

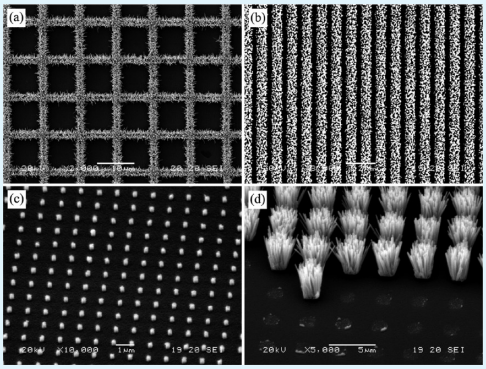

KEYWORDS: *ZnO nanorod arrays, electron beam lithography, hydrothermal growth, growth mechanism*

INTRODUCTION

Because of their unique optoelectronic properties and potential applications in optoelectronic devices, there has been a growing interest in the one-dimensional ZnO nanostructures, such as nanobelts, nanowires, and nanorods,[1,2] especially vertically aligned ZnO nanorod arrays are most attractive due to a variety of potential applications, ranging from light-emitting diodes (LED),[3] field-effect transistors,[4] photovoltaics,[5] and UV detectors[6] to gas sensors.[7] Each of these applications has different requirements in terms of geometry, density, position, and morphology of ZnO nanorod arrays for obtaining optimal performances. So fabricating ZnO nanorod arrays with precisely controlled morphology, alignment, and position is highly desired.

With this in view, patterned ZnO nanorod arrays have been achieved using various patterning methods including nanosphere lithography,[8] photolithography,[9] nanoimprint lithography[10,11] and e-beam lithography (EBL)[12] methods followed with a subsequent ZnO growth process. Among these, EBL is a promising method, which can fabricate various patterned structures with high precision ratio in nanometer-scales. Through this method, perfectly aligned and highly uniform ZnO arrays with controllable nanowires size and tunable pattern pitch were obtained by Xu et al.[13] In addition, the horizontally aligned ZnO arrays were also obtained with rather uniform in length and width by them.[14] By varying the aperture size defined by the EBL method, Cha-Hsin Chao et al.[15] obtained ZnO nanorods with different morphologies. It can be seen that the EBL can provide us a versatile way to control the position and morphology of the ZnO nanorod arrays. For the subsequent growth of vertically aligned ZnO nanorod arrays on prepatterned substrate, chemical vapor deposition (CVD),[16] pulse laser deposition (PLD),[17] and thermal evaporation[18] have been widely employed over the past years. Such methods are energy-consuming and expensive due to the high operation temperature and need the metal catalyst particles to guide the ZnO growth. In contrast, wet chemical methods are advantageous for their low temperature, facile manipulation, and large-scale fabrication, which have been widely used recently for the production of aligned ZnO nanostructures.[19−21]

The growth of patterned ZnO nanorod arrays combined the modern nanofabrication techniques and equipments with the subsequent solution-based hydrothermal growth have been reported by several research groups.[22,23] Until now, most research works focused on the growth of ZnO nanorod arrays with various morphology based on the prepatterned substrate. The precisely controlling the geometry, density, position and morphology of ZnO nanorod arrays with such a method is still a challenge due to the lack of understanding the parameters that affect their final morphology and the growth mechanisms during the hydrothermal growth process. In fact, the prepatterned geometry and the growth parameters such as seed layer, the precursor concentration, and the growth time have important influences on their final density, position and morphology. Therefore, understanding the relation between such parameters and their final morphology is significant to integrate such patterned ZnO nanorod arrays in various devices applications for an optional performance.

Received: February 27, 2012
Accepted: May 11, 2012
Published: May 21, 2012

   dx.doi.org/10.1021/am3003473 | *ACS Appl. Mater. Interfaces* 2012, 4, 2969−2977

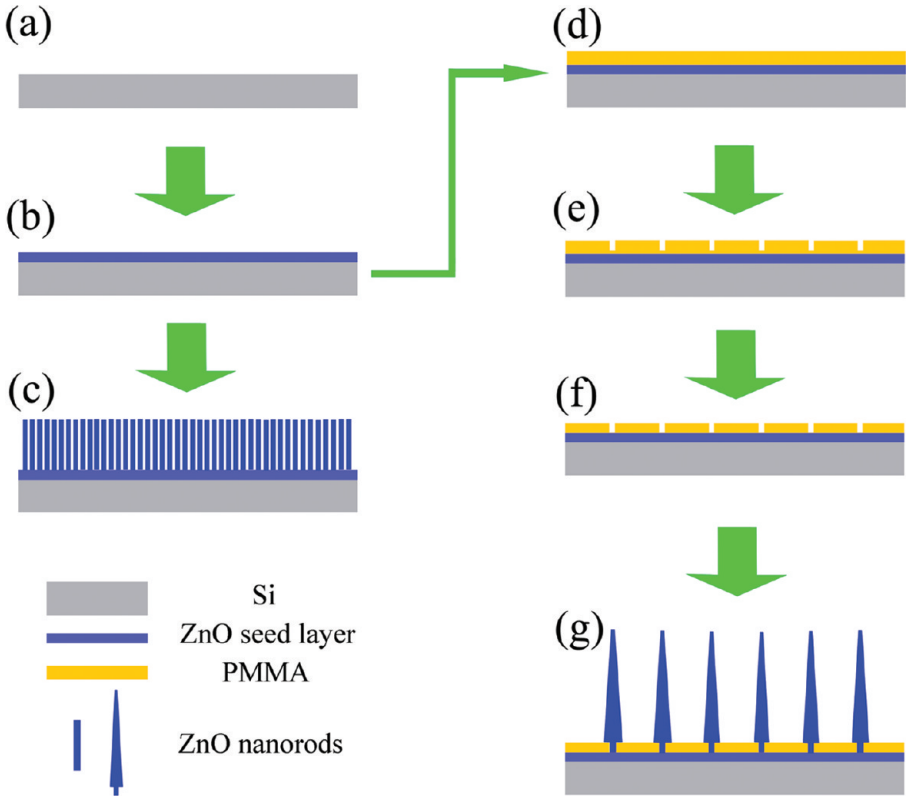

Figure 1. Schematic diagram of the fabrication and patterning process of ZnO nanorod arrays on Si substrate.

In this paper, ZnO nanorod arrays with different density and morphology were fabricated on the Si substrate by using the EBL and followed with the hydrothermal growth. The influence of the seed layers on the hydrothermal growth of ZnO nanorod arrays was investigated first. On this basis, the seed layer deposited at 300 °C was chosen for the subsequent hydrothermal process to obtain ZnO nanorod arrays with a uniform diameter distribution. The influences of the reaction time and the precursor concentration on the morphology of the ZnO nanorod arrays were also investigated. As the main controlling factor, EBL was used to fabricate the patterned ZnO seed areas with different size. Also, the growth mechanism was discussed in detail based on our experimental results. Finally, ZnO nanorod arrays with different morphology and density were achieved with high precision ratio on Si substrate using the hydrothermal growth, which was attractive for the potential applications in ZnO nanorod arrays-based nanodevices.

EXPERIMENTAL SECTION

All the chemicals were used as received without further purification. Zinc nitrate hexahydrate ($Zn(NO_3)_2{\cdot}6H_2O$) and hexamethylenetetramine (HMTA $(CH_2)_6N_4$) were purchased from Sigma Aldrich. Deionized water with a resistance of 18 MΩ cm^{-1} was obtained using a Milli-Q system (Millipore, Bedford, MA, USA). The schematic diagram of the processes was shown in Figure 1. Silicon (Si) wafers (100) used in experiments were cleaned sequentially with acetone, ethanol and deionized water for 10 min respectively, then dried with nitrogen flow (Figure 1a). ZnO seed layers were prepared using a commercial ion beam sputtering system (FDJ600, Shenyang Vacuum Equipment Factory, China). The sputtering was carried out using a ZnO target with 99.99% purity. A 3 cm diameter Kaufman ion source under an incidence of 45 ° to the target provided Ar ion for sputtering. The substrate was located parallel to the target holder. The base pressure was about 5×10^{-4} Pa, the working Ar pressure was 2.4×10^{-2} Pa and the flow rate was kept constant at 8 standard-state cubic centimeter per minute (sccm). The substrate temperature was controlled in the range of room temperature (RT 25 °C) to 500 °C by a heater under the sample substrate. All substrates were sputtered with the same time of 60 min. After that, hydrothermal treatment was carried out in a Teflon-lined stainless steel autoclave.

The substrate was placed upside down in a mixed aqueous solution of zinc nitrate hexahydrate ($Zn(NO_3)_2{\cdot}6H_2O$) and hexamethylenetetramine ($(CH_2)_6N_4$) with the same concentration (10 mM). The autoclave was sealed, and heated at 80 °C for the same time, then cooled in air. The samples were taken out of the solution, rinsed by deionized water, and then dried with N_2 flow, as shown in Figure 1c.

Patterned ZnO nanorod arrays were obtained by combining the low temperature hydrothermal growth method and the electron beam lithography (EBL) technique. First, photoresist solution of polymethylmethacrylate (PMMA) was spin-coated on the as-prepared ZnO seed layer, which resulting in a PMMA layer with a thickness of 320 nm (Figure 1d). Next, a DY-2000A electrons beam lithography (EBL) system based on JEOL 5600 scanning electron microscopy was used to write the desired patterns on the PMMA photoresist layer above the ZnO seed layer (Figure 1e). After the developing process, the residue layer of PMMA pattern was removed by reactive ion etching (Trion Phontom, USA). Finally, selectively grown ZnO nanorod arrays were obtained via the hydrothermal method above as shown in Figure 1g. After the hydrothermal growth, the PMMA photoresist layer was dissolved by putting the substrate into acetone for 1 min.

Surface morphology measurements of deposited ZnO seed layers were performed using an atomic force microscope (AFM, Seiko SPA400, Japan). The crystalline structure of the samples was characterized by an X-ray diffractometer (X'Pert Pro PW3040/60, Holland). The morphologies of the ZnO nanorod arrays were characterized by scanning electron microscopy (SEM, JEOL 5600). Transmission electron microscope (TEM), high-resolution TEM (HRTEM) images, and selected area electron diffraction (SAED) patterns were obtained on a JEOL JEM-2010.

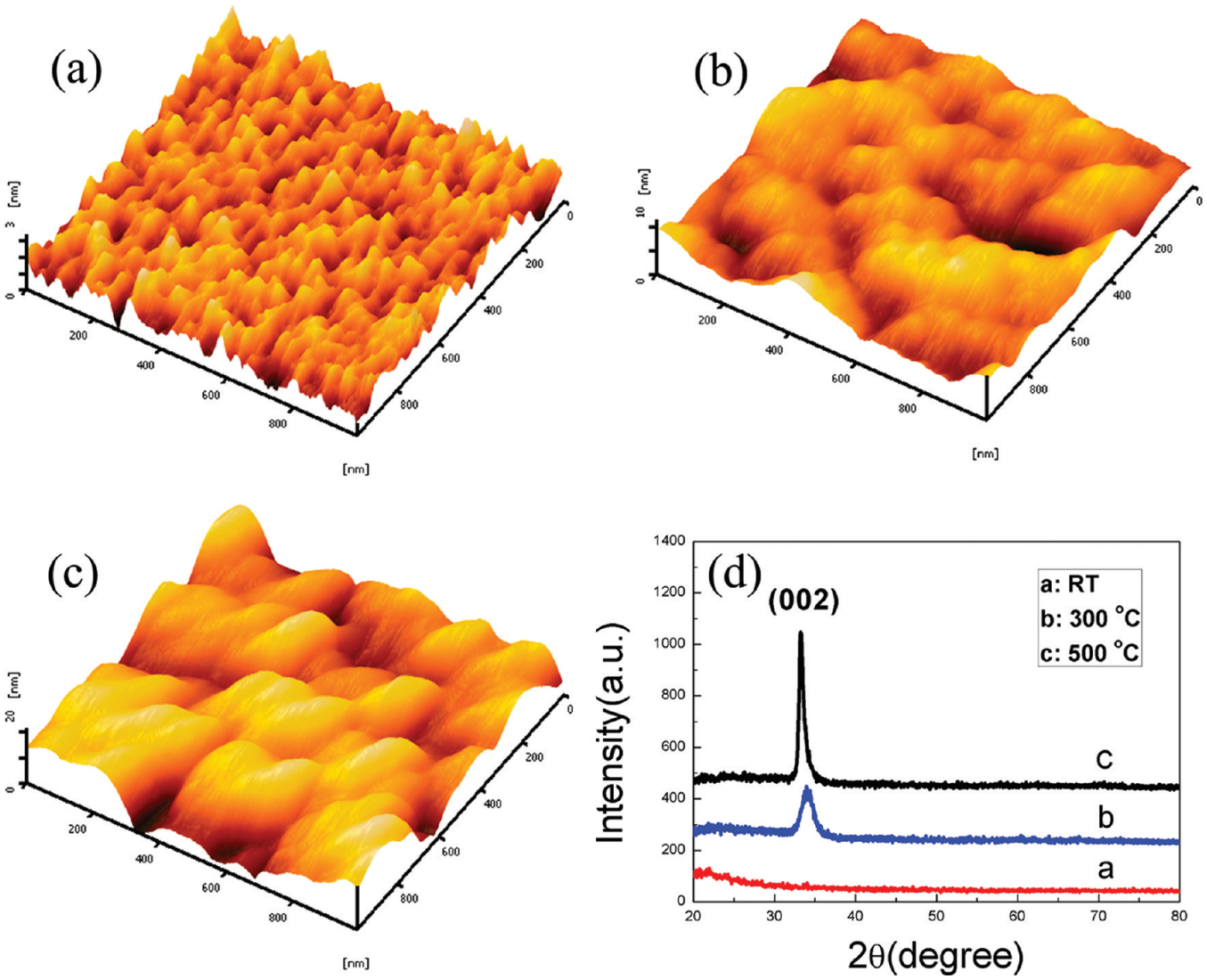

Figure 2. (a–c) AFM morphologies and (d) XRD patterns of ZnO seed layers obtained at different deposition temperatures: (a) room temperature, (b) 300 °C, (c) 500 °C.

RESULTS AND DISCUSSION

Characterization of the ZnO Nanorod Arrays. Generally, a ZnO seed layer should be prepared before the growth of well-aligned ZnO nanorods by the hydrothermal method, which has great impact on the morphology and the density of the rod array structures.[24,25] By adjusting the parameter just like the crystalline structures of the seed layers, ZnO nanorod arrays with various morphology and density will be obtained. In this experiment, ion beam sputtering deposition methods was used to control the crystalline structures of the seed layers by changing the deposition temperature during the sputtering process. And then, the influence of the deposited ZnO seed layers on the morphology of the ZnO nanorod arrays in the hydrothermal process was investigated. The substrate temperature in the ion beam deposition process plays an important role in determining the surface morphology and crystalline structure of ZnO seed layers.[26,27] Figure 2a–c showed the three-dimensional AFM images of ZnO seed layers deposited on silicon wafer with the different substrate temperatures of room temperature (RT 25 °C), 300 °C, and 500 °C. It indicated that the size of grains had a noticeable change with increasing the substrate temperatures from RT to 500 °C. Figure 2a presents the morphology of the ZnO seed layer deposited at room temperature, showing a surface covered with small amorphous particles with a typical root-mean-square (rms) roughness of 0.403 nm. With higher substrate temperature, the densely packed small particles had much more energy to merge into large crystalline grains and the surface defects at the grain boundaries were reduced also. The rms roughness of ZnO seed layer deposited at the substrate temperature of 300 and 500 °C were 2.402 and 3.751 nm, respectively. The quality of ZnO seed layer was improved because of the redistribution of crystalline grain by heating the substrate during the ion beam deposition process.

Figure 2d was the corresponding XRD patterns of ZnO seed layer deposited with various substrate temperatures. When the ZnO seed layers were deposited at RT, there was no obvious peak, which indicated the typical amorphous characters of the ZnO film. With the substrate temperatures increased to 300 °C, an obvious single (002) diffraction peak at 2θ = 34.38° corresponding to ZnO wurtzite structure with high *c*-axis orientation was obtained. And diffraction peak with higher intensity appeared on 500 °C films which indicated that the crystallinity and *c*-axis orientation of ZnO seed layers were

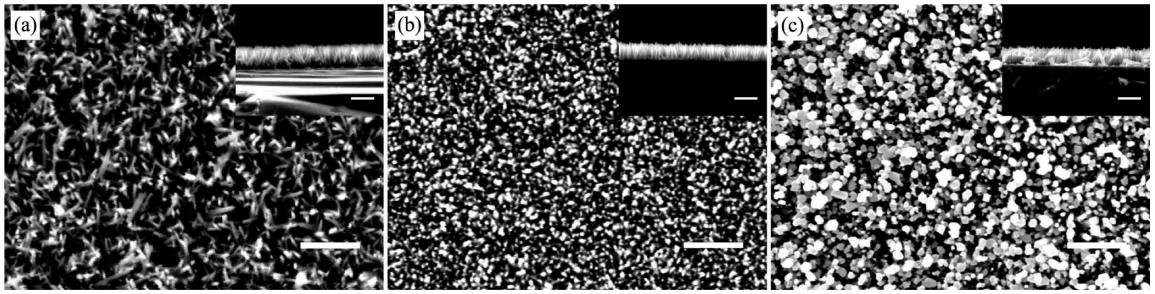

Figure 3. SEM images of the ZnO nanorod arrays grown on the seed layers at deposition temperatures: (a) room temperature, (b) 300 °C, (c) 500 °C. The scale bars correspond to 2 μm.

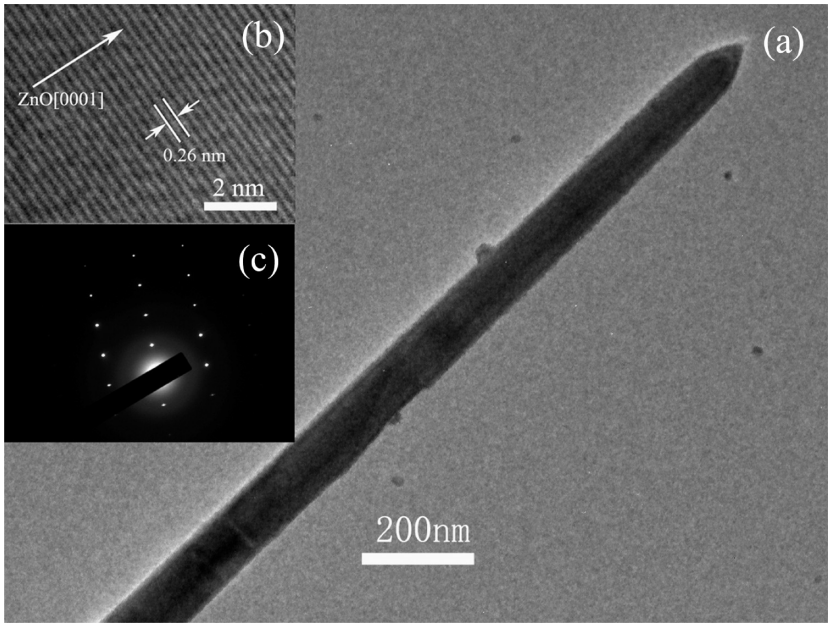

Figure 4. (a) TEM and (b) HRTEM images and (c) SAED pattern of ZnO nanorod grown on the ZnO seed layer deposited at 300 °C.

improved effectively with the enhanced supplying of thermal energy in the ion beam deposition process.

Figure 3 shows the SEM images of the ZnO nanorod arrays grown under the same hydrothermal conditions with the substrate temperature of RT, 300 °C, and 500 °C, respectively. The insets as shown in Figure 3 are the cross-sectional images of the ZnO nanorod arrays. During the hydrothermal reaction process, the concentration of zinc nitrate hexahydrate ($Zn(NO_3)_2{\cdot}6H_2O$) and hexamethylenetetramine ($(CH_2)_6N_4$) were both 10 mM. The growth temperature was 80 °C and the growth time was 12 h. From Figure 3(a), we can see that the ZnO nanorod array was grown on the ZnO seed layer with a broad diameter distribution from 50−200 nm and a length of about 1000 nm. The nucleation and growth of ZnO nanorods were random oriented with wide diameter distributions due to the amorphous structure and poor preferred orientation of the seed layers. Figure 3b showed that highly dense ZnO nanorods perpendicular to the substrate with a fairly small diameter deviation were uniformly distributed on the Si substrate. Under the higher deposition temperature, a larger diameter of the ZnO nanorod with some particles on the rod arrays was observed in Figure 3b. The higher deposition temperature led to the particles merge together and formed larger ZnO seed grains, which caused the nanorods to grow with larger diameter and a large variation in width.

Figure 4a was the TEM image of a single ZnO nanorod grown on the ZnO seed layer deposited at 300 °C. The nanorod had a uniform diameter of about 100 nm. The insert HRTEM image of Figure 4b indicated that well-defined lattice fringe separation with 0.26 nm which was corresponding to the distance between two (0002) crystal planes of the wurtzite hexagonal ZnO. It was also in agreement with the selected area electron diffraction (SAED) results (the inset of Figure 4c), which indicated that the nanorod had a high quality single-crystalline structure and growth along the [0001] direction.

From above analysis, well-aligned ZnO nanorod arrays were successfully synthesized with controllable morphology and density on Si wafers. The ZnO seed layer deposition temperature had a great influence on the final morphology of the ZnO nanorod arrays. The nanorod arrays grown on seed layer prepared at 300 °C had the better alignment and diameter variation than the other two substrates. Therefore, the 300 °C seed layer preparation process was chosen for the following patterned ZnO nanorod arrays growth.

Controllable Growth of Patterned ZnO Nanorod Arrays with Different Morphology. Patterned ZnO nanorod arrays were fabricated by using EBL method combined with the hydrothermal reaction process. The influence of the precursor concentration on the morphology of the patterned ZnO nanorod arrays was investigated. A series of experiments

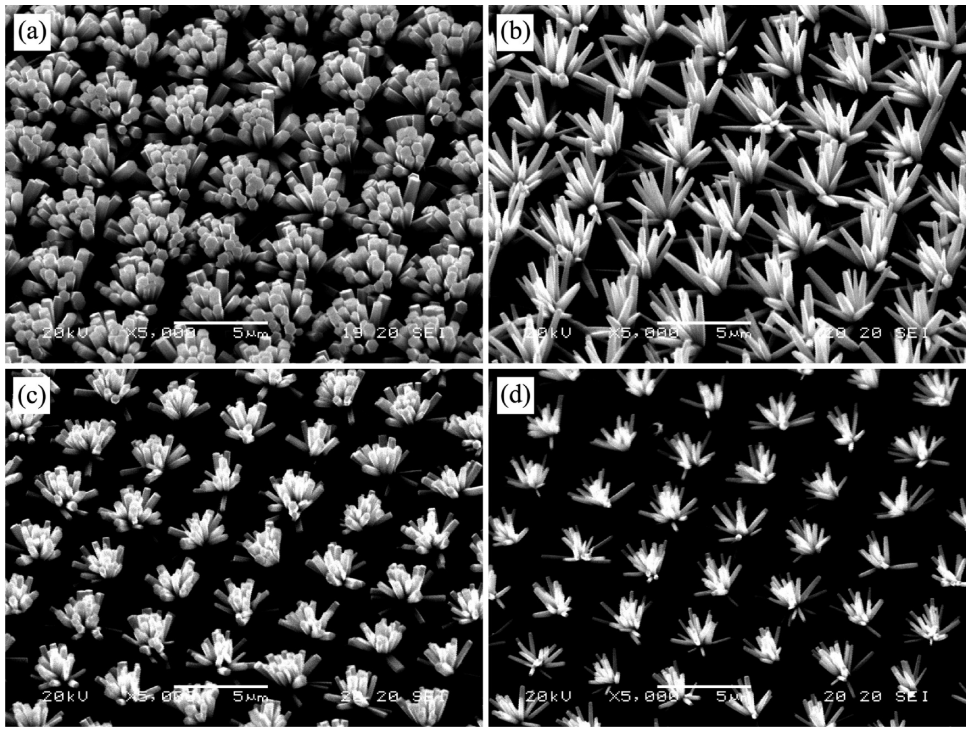

Figure 5. SEM images of ZnO nanorod arrays grown in different precursor concentration: (a) 40, (b) 20, (c) 10, (d) 5 mM.

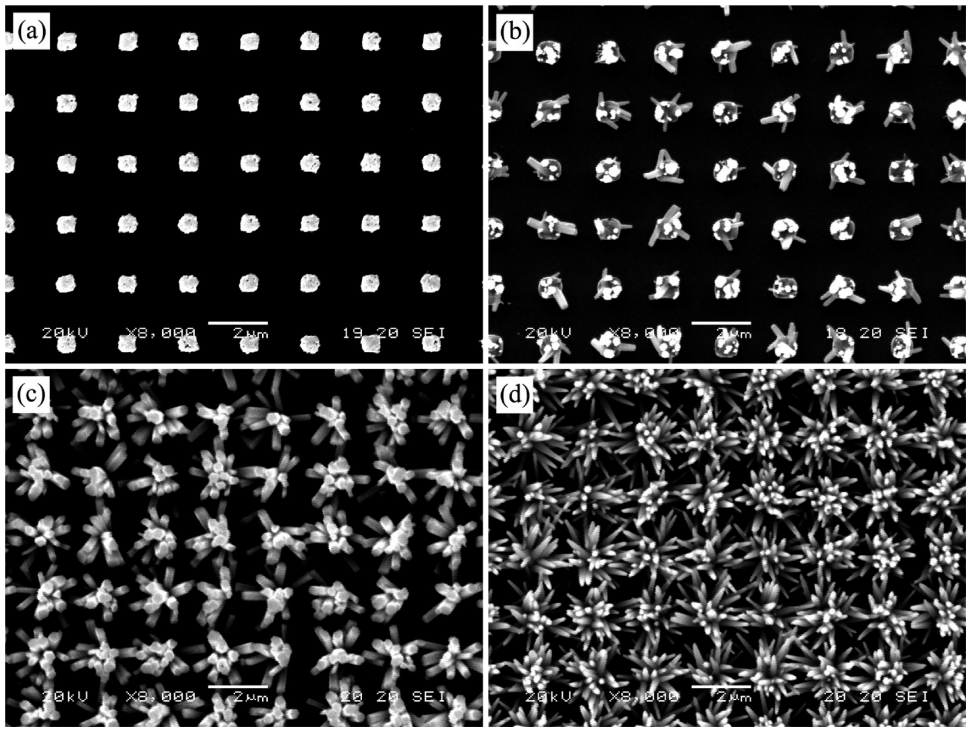

Figure 6. SEM images of ZnO nanorod arrays obtained at different growth time: (a) 100, (b) 150, (c) 360, and (d) 720 min.

were performed by varying the precursor concentration while keeping the same reaction temperature (80 °C) and growth time (6 h). The typical patterns created by the EBL methods were aperture arrays with a feature size of 350 nm and spacing distance of 2 μm. Figure 5 showed the SEM images of ZnO nanorod arrays grown with different precursor concentration ranging from 5 to 40 mM. Patterned ZnO nanorod arrays were successfully obtained, which confined strictly to the preformed ZnO seed areas. The diameter and the density of ZnO nanorods increased with the increasing of precursor concentration during the hydrothermal reaction process as shown in Figure 5a–d. The density of ZnO nanorods could be controlled by the initial concentrations of the zinc salt and HMTA which had been investigated in detail by Xu et al.[28] Their results showed that the precursor concentration had an influence on the density of ZnO nanorod arrays due to the number of nuclei

dx.doi.org/10.1021/am3003473 | ACS Appl. Mater. Interfaces 2012, 4, 2969–2977

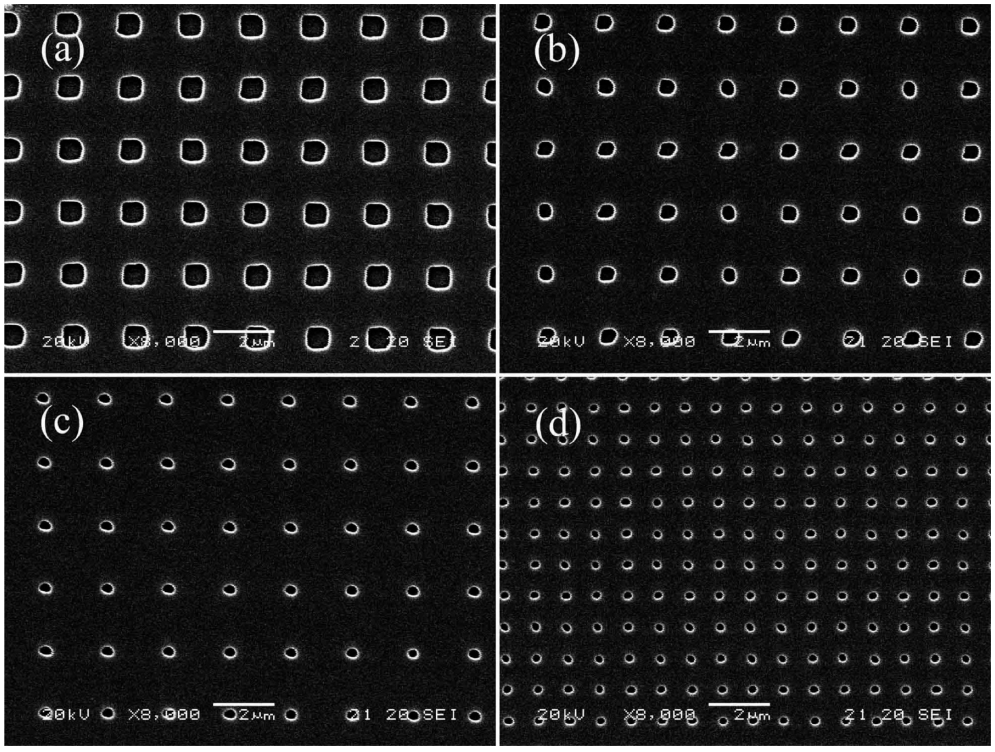

Figure 7. SEM images of two-dimensional periodic PMMA aperture arrays with different feature sizes: (a) 700, (b) 350, (c) 200, (d) 150 nm. The period of the aperture is 2 μm.

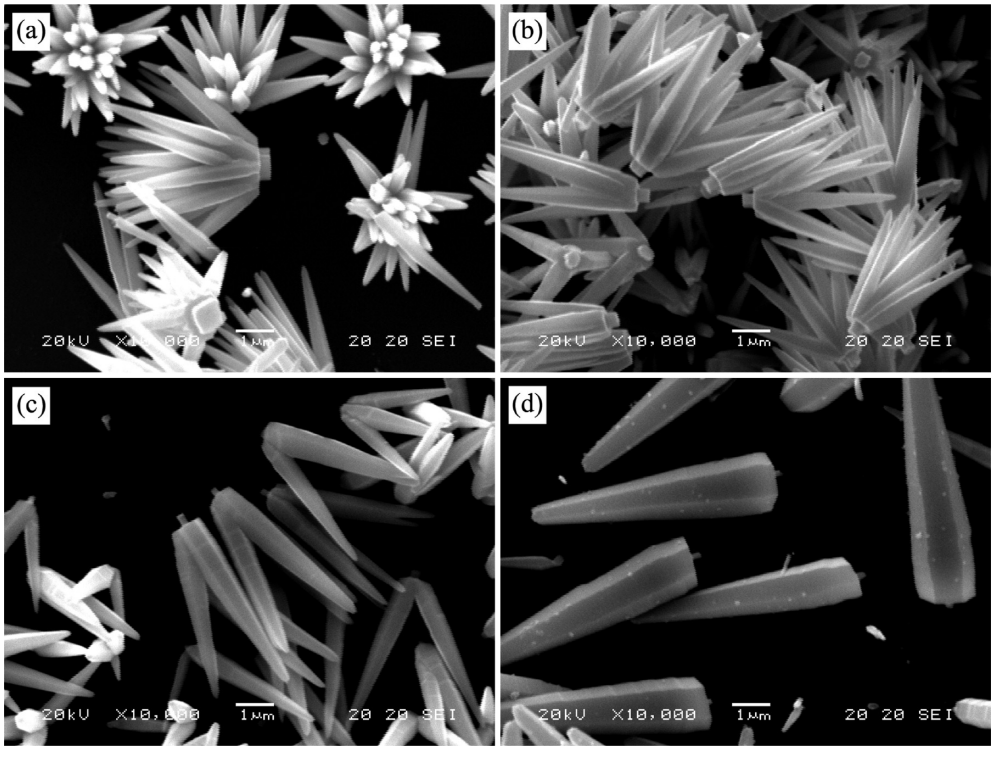

Figure 8. SEM images of ZnO nanorod arrays obtained at different PMMA apertures: (a) 700, (b) 350, (c) 200, and (d) 150 nm.

formed at the beginning of the nanorod growth was different. In our experiment, since the size of the ZnO seed areas was predefined, so the number of nucleation at the beginning of the nanorod growth was determined. At higher precursor concentration, more Zn^{2+} supplied in the solution would make the lateral growth of the ZnO nanorod. This would cause the diameter of the rod increased and subsequently had a density variation on the seed areas.

Since the growth time during the hydrothermal process was another controlling factor, the morphology variations of ZnO nanorod arrays were also investigated for the different growth time. Figure 6 showed the SEM images of ZnO nanorod arrays

dx.doi.org/10.1021/am3003473 | ACS Appl. Mater. Interfaces 2012, 4, 2969−2977

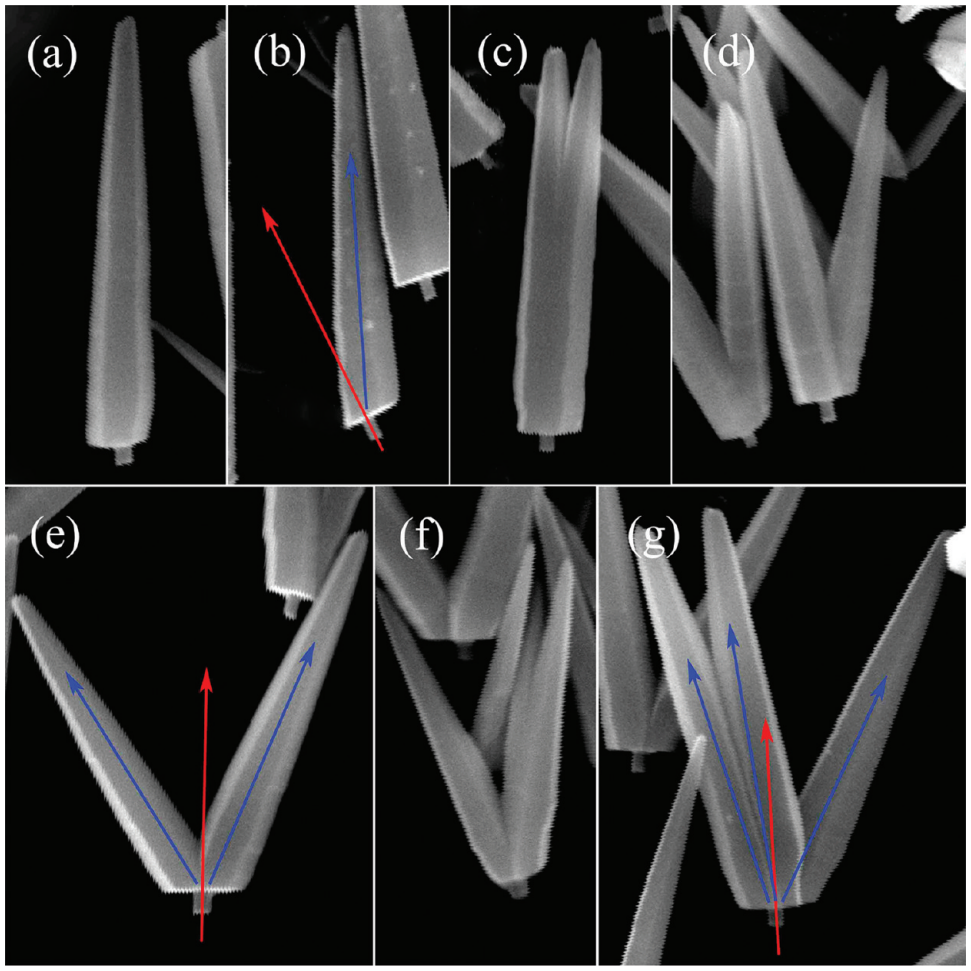

Figure 9. SEM images of various ZnO nanorods grown on the ZnO columns: (a, b) single nanorod, (c−e) double nanorods, (f, g) ternary nanorods.

with different growth time, which kept the same precursor concentration (10 mM) and growth temperature (80 °C). From Figure 6a, we could see that the column like ZnO was formed on the seed areas at the beginning of the hydrothermal process with the 100 min growth time. With the growth time increased to 150 min, few ZnO nanorods were grown from the column like ZnO area in the seed areas as shown in Figure 6b. More ZnO nanorods were formed when the growth time was increased to 6 h (Figure 6c). With a further increase in the growth time to 12 h, the diameter of the nanorod was decreased and much larger density nanorod arrays were obtained as shown in Figure 6d. In fact, the growth processes could be separated into two stages during the formation ZnO nanorod arrays. The first process was the ZnO growth in PMMA aperture areas. Then the ZnO nanorods grew epitaxially onto the ZnO seed layer with *c*-axis orientation in the precursor solution. By the confinement of the PMMA photoresist, the ZnO crystals suffered the physical constraints of the preformed patterns. Therefore it could only grow into the column-like morphology as we observed in Figure 6a. As the reaction proceed, the ZnO nanostructures grew epitaxially from different nucleation sites on the column, which led to the growth along different direction as observed in Figure 6b. With the further increase in the reaction time, the concentration of Zn^{2+} and OH^{-} ions in the solution was decreased, which resulted in the growth speed of lateral growth slowed down faster than that of the *c*-axis growth. This caused the diameter decrease and density increase of the ZnO nanorod arrays as observed in Figure 6d.

Morphology Control of Patterned ZnO Nanorod Arrays with Different Feature Size of PMMA Holes. As the main controlling factor on the patterned ZnO nanorod arrays, EBL was used to fabricate the seed areas with different size. Figure 7 showed the SEM images of two-dimensional periodic PMMA aperture arrays with different feature size ranging from 700 to 150 nm. After removing the residue layer of photoresist by reactive ion etching, ZnO nanorod arrays were achieved after the same hydrothermal process. The precursor concentration was kept at 10 mM. The growth temperature was kept at 80 °C, and the growth time was 12 h. ZnO nanorod arrays with different morphology were obtained on different PMMA aperture fabricated by EBL method as shown in Figure 8. To investigate the formation mechanisms of the ZnO nanorod arrays, the rods were scraped off the substrate for further observation. The number of the ZnO nanorods grew from one aperture were about 35, 8, and 2 for the 700, 350, and 200 nm photoresist apertures, respectively. Further reduced the aperture size to 150 nm, the individual ZnO nanorod could be obtained as shown in Figure 8d. The number of ZnO nanorods in one PMMA aperture reduced with the aperture size decreased. The average diameter and length of the ZnO nanorods increased obviously with the decrease of the aperture size as shown in Figure 8a−d. We should note that there was an abrupt increase in rod size as shown from panels c and d in

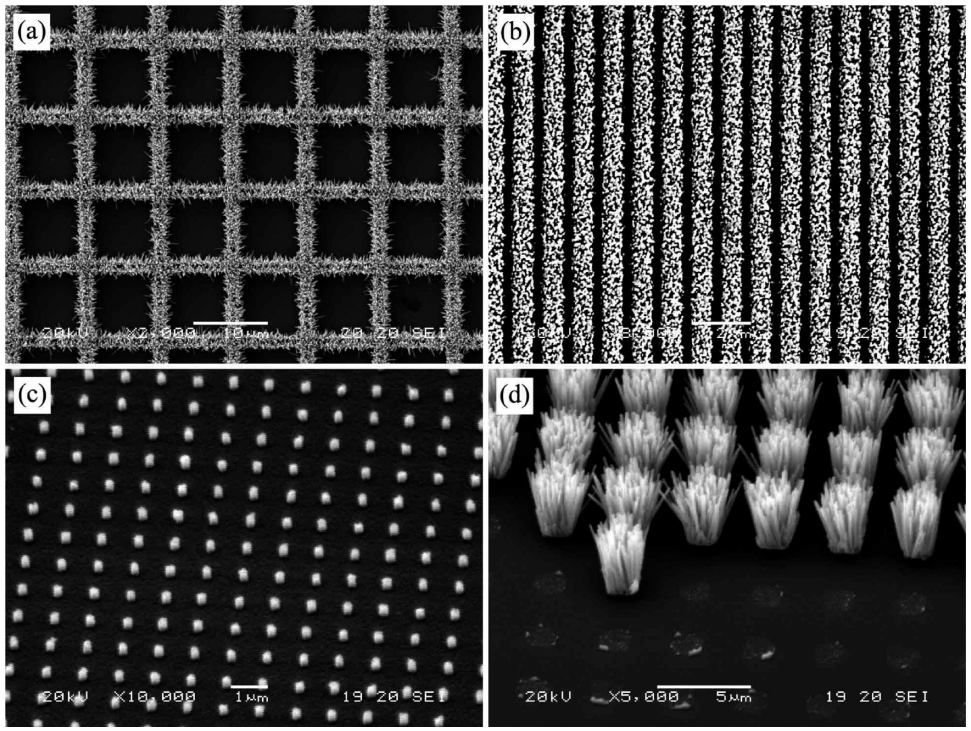

Figure 10. SEM images of various patterned ZnO nanorod arrays: (a) Top view of the double line ZnO nanorod grid with 2.5 μm line width and period of 10 μm, (b) paralleled ZnO nanorod lines with 600 nm width and 1 μm period, (c) 45° tilt view of individual ZnO nanorod arrays with diameter of 250 nm and period of 1 μm, (d) patterned ZnO nanorod arrays with 1 μm feature size and 4 μm period.

Figure 8. The diameter of the nanorod grew in the 150 nm aperture were three times larger than that of grew in 200 nm aperture. For the larger PMMA aperture, more nucleation sites would form to guide the growth of the ZnO nanorod arrays. Therefore, more ZnO nanorods were obtained in one aperture. For the larger density ZnO nanorods in the hydrothermal reaction process, ZnO nanorods competed with each other, each nanorod got fewer nutrients, which resulted in the smaller diameter of nanorod compared with the lower density of the ZnO nanorod arrays.

It was noted that all of the ZnO nanostructures had a column structure at the bottom of the rod arrays. And these columns had the same diameter with the PMMA aperture size. ZnO nanorods which grew epitaxially on the top of column had a radiate spatial orientation. The size of ZnO nanorod arrays was not equal to the aperture size. It was even larger than the opening size of the aperture when the aperture size was small enough. In order to observe this phenomenon in detail, ZnO nanorods grown in PMMA aperture with the feature size of 150 and 200 nm were selected for further investigation as shown in Figure 9. It was interesting to note that the growth orientations of the column and ZnO nanorod were different as shown in images a and b in Figure 9. The angle between the axial orientation of single ZnO nanorod and the normal to the substrate was about 23 ° as shown in Figure 9b. However, only 5 ° was observed in Figure 9a. Usually, the column structure of ZnO was physically constrained by the patterns of the polymers. Therefore, the axial orientation was aligned vertical to the substrate. When the diameter of photoresist aperture was 150 nm, the photoresist window was smaller than the grain size in the seed layer, the single crystalline column would be formed in the aperture which had the same (002) crystal orientation with the seed layer. As the hydrothermal process proceeded, individual ZnO would be formed on the ZnO columns. With the larger photoresist window of 200 nm in diameter, there were more ZnO seeds in the photoresist aperture which resulted in the two or three ZnO nanorods grew out of the aperture. The angles between them were determined by the divergence of the crystallographic orientations of the original grains on the ZnO seed layers. Figure 9c–e were the ZnO clusters of two nanorods with different angles. Figure 9f–i showed the ZnO clusters containing three nanorods. In the addition, when the feature size of the PMMA window increased larger, the ZnO clusters with multinanorods could be obtained.

Patterned Growth of ZnO Nanorod Arrays with Different Morphology by Combining the EBL and Hydrothermal Growth Method. By controlling the parameter of the EBL and the hydrothermal method together, ZnO nanostructures with different morphology were fabricated for various purposes of future ZnO nanorod arrays based nanodevices. Figure 10a showed the double line ZnO nanorods grid with a 2.5 μm line width and a period of 10 μm. The precursor concentration was 5 mM and the growth time was 12 h in the hydrothermal process. Paralleled ZnO nanorods lines were also fabricated as shown in Figure 10b, the width was 600 nm and the period was 1 μm. The hydrothermal condition was 20 mM concentration precursor solution with 180 min reaction time. Figure 10c presented the SEM images of 45 ° tilt view of individual ZnO nanorod arrays with a diameter of 250 nm and a period of 1 μm. The precursor concentration was 5 mM, the growth time was 150 min. After 24 h of hydrothermal reaction in 5 mM precursor solution, high aspect ratio patterned ZnO nanorod arrays were obtained as shown in Figure 10d. The average diameter and length of the ZnO nanorods were about 120 and 3000 nm, respectively. And the feature size of the pattern was 1.5 μm with a spacing distance about 4 μm.

CONCLUSION

In conclusion, we have demonstrated controllable fabrication of ZnO nanorod arrays with different geometric parameters through the combination of EBL and hydrothermal growth process. The seed layer prepared at 300 °C was chosen for the hydrothermal growth in order to obtain ZnO nanorod arrays with a uniform size distribution. In the hydrothermal reaction process, the density and the diameter of patterned ZnO nanorod arrays became larger with the increasing of the precursor concentration. Meanwhile, the diameter would become smaller and the density of ZnO nanorod arrays would become larger with longer reaction time. Different sizes of the aperture were fabricated by using EBL method for regulated the seed areas of ZnO nanorod arrays. It is interesting to note that the diameter of the ZnO nanorod was larger than the size of the PMMA aperture with diameter about 150 nm. The morphology of ZnO nanorod arrays was found to be strongly dependent on the opening holes made by EBL method. Understanding the parameters that affect the final morphology and the growth mechanisms was important for potential applications in ZnO nanorod array-based nanodevices.

AUTHOR INFORMATION

Corresponding Author

*E-mail: zld@henu.edu.cn.

Present Address

D.Z. and S.W. contributed equally to this paper.

Notes

The authors declare no competing financial interest.

ACKNOWLEDGMENTS

This work was supported by the National Natural Science Foundation of China (Grants 20903034 and 10874040), and the Cultivation Fund of the Key Scientific and Technical Innovation Project, Ministry of Education of China (708062).

REFERENCES

(1) Ozgür, U.; Alivov, Ya. I..; Liu, C.; Teke, A.; Reshchikov, M.; Dogan, S.; Avrutin, V.; Cho, S. J.; Morkoc, H. *J. Appl. Phys.* **2005**, *98*, 041301.
(2) Djurisic, A. B.; Ng, A. M. C.; Chen, X. Y. *Prog. Quantum Electron.* **2010**, *34*, 191−259.
(3) Park, H.; Byeon, K. J.; Yang, K. Y.; Cho, J. Y.; Lee, H. *Nanotechnology* **2010**, *21*, 355304.
(4) Ahsanulhaq, Q.; Kim, J. H.; Hahn, Y. B. *Nanotechnology* **2007**, *18*, 485307.
(5) Xu, C. K.; Wu, J. M.; Desai, U. V.; Gao, D. *J. Am. Chem. Soc.* **2011**, *133*, 8122−8125.
(6) Hsu, C. H.; Chen, D. H. *Nanotechnology* **2010**, *21*, 285603.
(7) Jha, S. K.; Liu, C. P.; Chen, Z. H.; Chen, K. J.; Bello, I.; Zapien, J. A.; Zhang, W. J.; Lee, S. T. *J. Phys. Chem. C* **2010**, *114*, 7999−8004.
(8) Dong, J. J.; Zhang, X. W.; Yin, Z. G.; Zhang, S. G.; Wang, J. X.; Tan, H. R.; Gao, Y.; Si, F. T.; Gao, H. L. *ACS Appl. Mater. Interfaces* **2011**, *3*, 4388−4395.
(9) Kim, T. U.; Kim, J. A.; Pawar, S. M.; Moon, J. H.; Kim, J. H. *Cryst. Growth Des.* **2010**, *10*, 4256−4261.
(10) Kang, H. W.; Yeo, J.; Hwang, J. O.; Hong, S.; Lee, P.; Han, S. Y.; Lee, J. H.; Rho, Y. S.; Kim, S. O.; Ko, S. H.; Sung, H. J. *J. Phys. Chem. C* **2011**, *115*, 11435−11441.
(11) George, A.; Maijenburg, A. W.; Maas, M. G.; Blank, D. H. A.; Elshof, J. E. *Langmuir* **2011**, *27*, 12235−12242.
(12) Yong-Jin, K.; Chul-Ho, L.; Young Joon, H.; Gyu-Chul, Y.; Sung Soo, K.; Hyeonsik, C. *Appl. Phys. Lett.* **2006**, *89*, 163128.
(13) Xu, S.; Wei, Y. G.; Kirkham, M.; Liu, J.; Mai, W. J.; Davidovic, D.; Snyder, R. L.; Wang, Z. L. *J. Am. Chem. Soc.* **2008**, *130*, 14958−14959.
(14) Xu, S.; Ding, Y.; Wei, Y. G.; Fang, H.; Shen, Y.; Sood, A. K.; Polla, D. L.; Wang, Z. L. *J. Am. Chem. Soc.* **2008**, *131*, 6670−6671.
(15) Chao, C. H.; Huang, J. S.; Lin, C. F. *J. Phys. Chem. C* **2009**, *113*, 512−517.
(16) Fragala, M. E.; Satriano, C.; Aleeva, Y.; Malandrino, G. *Thin Solid Films* **2010**, *518*, 4484−4488.
(17) Liu, Z. W.; Ong, C. K.; Yu, T.; Shen, Z. X. *Appl. Phys. Lett.* **2006**, *88*, 053110.
(18) Umar, A.; Karunagaran, B.; Suh, E. K.; Hahn, Y. B. *Nanotechnology* **2006**, *17*, 4072−4077.
(19) Liu, W. B.; Hu, G. D.; Cui, S. G.; Zhou, Y.; Wu, H. T. *Cryst. Growth Des.* **2008**, *8*, 4014−4020.
(20) Qin, Z.; Liao, Q. L.; Huang, Y. H.; Tang, L. D.; Zhang, X. H.; Zhang, Y. *Mater. Chem. Phys.* **2010**, *123*, 811−815.
(21) Kenanakis, G.; Vernardou, D.; Koudoumas, E.; Katsarakis, N. *J. Cryst. Growth* **2009**, *311*, 4799−4804.
(22) Li, C.; Hong, G. S.; Wang, P. W.; Yu, D. P.; Qi, L. M. *Chem. Mater.* **2009**, *21*, 891−897.
(23) Weintraub, B.; Zhou, Z. Z.; Li, Y. H.; Deng, Y. L. *Nanoscale* **2010**, *2*, 1573−1587.
(24) Song, J. J.; Lim, S. W. *J. Phys. Chem. C* **2007**, *111*, 596−600.
(25) Giri, P. K.; Dhara, S.; Chakraborty, R. *Mater. Chem. Phys.* **2010**, *122*, 18−22.
(26) Gessert, T. A.; Coutts, T. L.; Noufi, R. *J. Vac. Sci. Technol. A* **1994**, *12*, 1507−1512.
(27) Tsai, H. Y. *J. Mater. Proc. Technol.* **2007**, *192−193*, 55−59.
(28) Xu, S.; Lao, C. S.; Weintraub, B.; Wang, Z. L. *J. Mater. Res.* **2008**, *23*, 2072−2077.